Published in final edited form as:
Small. 2008 November ; 4(11): 1925–1929. doi:10.1002/smll.200800261.

Metallic Iron Nanoparticles for MRI Contrast Enhancement and Local Hyperthermia**

Costas G. Hadjipanayis*,
Department of Neurological Surgery, Winship Cancer Institute, Emory University School of Medicine, Atlanta, GA 30322 (USA), E-mail: chadjip@emory.edu

Michael J. Bonder,
Magnetics Laboratory, Department of Physics and Astronomy, University of Delaware, Newark, DE 19716 (USA)

Srinivasan Balakrishnan,
Magnetics Laboratory, Department of Physics and Astronomy, University of Delaware, Newark, DE 19716 (USA)

Xiaoxia Wang,
Department of Radiology, Emory University School of Medicine, Atlanta, GA 30322 (USA)

Hui Mao, and
Department of Radiology, Emory University School of Medicine, Atlanta, GA 30322 (USA)

George C. Hadjipanayis
Magnetics Laboratory, Department of Physics and Astronomy, University of Delaware, Newark, DE 19716 (USA)

Keywords

hyperthermia; magnetic nanoparticles; poly(ethylene glycol); relaxation times

Current magnetic-nanoparticle technology is challenging due to the limited magnetic properties of iron oxide nanoparticles (IONPs). Increasing the saturation magnetization of magnetic nanoparticles may permit more effective development of multifunctional agents for simultaneous targeted cell delivery, magnetic resonance imaging (MRI) contrast enhancement, and targeted cancer therapy in the form of local hyperthermia. We describe the synthesis and characterization of novel iron-based nanoparticles (FeNPs) coated with biocompatible bis-carboxyl-terminated poly(ethylene glycol) (cPEG). In comparison to conventional IONPs similar in size (10 nm), FeNPs particles have a much greater magnetization and coercivity based on hysteresis loops from sample magnetometry. Increased magnetization afforded by the FeNPs permits more effective generation of local hyperthermia than IONPs when subjected to an oscillating magnetic field in a safe frequency range. Furthermore, FeNPs have a much stronger shortening effect on T_2 relaxation time than IONPs, suggesting that FeNPs may be more effective MRI contrast agents. Next-generation FeNPs with a biocompatible coating may

**This work was supported in part by grants from the Georgia Cancer Coalition, Distinguished Cancer Clinicians and Scientists Program (C. G. H.), NIH Center for Cancer Nanotechnology in Excellence Program (H. M.), EmTech Bio, Inc (H. M.), and NSF DMR 0302544 (G. C. H.).

*Prof. C. G. Hadjipanayis, Department of Neurological Surgery, Winship Cancer Institute, Emory University School of Medicine, Atlanta, GA 30322 (USA), E-mail: E-mail: chadjip@emory.edu.

in the future be functionalized with the attachment of peptides specific to cancer cells for imaging and therapy in the form of local hyperthermia.

The diagnostic and therapeutic advantages of magnetic nanoparticles stem from the static and dynamic magnetism of the nanoparticles along with the ability to impart cell-specific functionality. Biocompatibility of such nanomaterials allows for in vivo applications in animals and humans. Currently, various formulations of IONPs have been developed for drug-delivery schemes,[1,2] magnetic cell separation and cell targeting,[3,4] MRI contrast enhancement, [5–13] and hyperthermia treatment of cancer.[14–16] Magnetic nanoparticles provide localized changes of longitudinal and transverse relaxation times of water and field inhomogeneities to improve the contrast of MRI.[17] When magnetic nanoparticles are subjected to an alternating current (AC) field, the resulting eddy current, hysteresis, and Brownian rotational losses can provide a nanoscale source of heat capable of imparting cell death.[18,19] The ability to combine MRI contrast enhancement and therapy in the form of hyperthermia as well as the possibility of functionalizing particles specific to biomarkers may further advance the use of magnetic nanoparticles in biomedical research and eventually in clinical applications. However, the above technologies are not fulfilled or optimized by using currently available IONPs. Due to their oxidized state, IONPs have a limited saturation magnetization. In principle, greater saturation magnetization may insure accurate dosing due to increased interaction with applied magnetic fields. The force a nanoparticle experiences when subjected to a magnetic field is linearly proportional to the magnetic moment *(m)* of the particle, such that, $\vec{F} = (\vec{m} \cdot \vec{\nabla})\vec{B}$, where $\vec{B}$ is the magnetic induction given by $\vec{B} = \mu\vec{H} + 4\pi\vec{M}$, where $\vec{H}$ is an inhomogeneous magnetic field, $\vec{M}$ is the magnetization, and μ is the magnetic permeability. Therefore, for a fixed field gradient $\vec{B}$, a higher magnetization imparts a greater force on the nanoparticle. In addition, since the strength of the stray fields from a nanoparticle is proportional to its magnetization, stronger stray fields may reduce the relaxation times of surrounding water molecules and provide greater MRI contrast. Nanoparticles with larger magnetization may also provide lower excitation frequencies than IONPs since their ferromagnetic resonance (FMR) frequency is lower due to lower magneto-crystalline anisotropy.[20] As a result, hyperthermia treatments can be administered at a safe biological frequency range ($f < 1.2$ MHz). In principle, nanoparticles composed of elemental iron may provide greater magnetization than IONPs. Although nanoparticles made from elemental Fe may be highly reactive in an aqueous environment, issues of biocompatibility, solubility, and stability can be addressed by coating the nanoparticles with an inert polymer such as PEG.[21] In addition to passivating the surface, a biocompatible PEG coating may provide a method to overcome size restrictions by limiting particle growth[22] and also permit surface functionalization for conjugating bioactive ligands.

In this study, we report on the synthesis and characterization of bis-carboxyl-terminated PEG-coated FeNPs with magnetization greater than that of IONPs with comparable particle size. Comparison studies between the novel FeNPs and conventional IONPs were performed using vibrating-sample magnetometry, MRI relaxometry, and temperature measurements during AC field excitation. Synthesis of the FeNPs was performed by the optimized chemical reduction of ferrous chloride with sodium borohydride in a junction using a 1.7 molar ratio, as shown in Equation (1), to maximize the Fe content.

$$(FeCl_2 + Ethanol) + (NaBH_4 + H_2O) \Rightarrow Fe(B) + NaCl + H_2 + Ethanol + H_2O \quad (1)$$

Immediately upon synthesis, the nanoparticles are quenched in a bis-carboxyl-terminated PEG (cPEG) and ethanol solution to provide their biocompatible coating. In this synthesis procedure, FeNPs with a mean particle diameter of around 10nm and a standard deviation of 2nm are

formed with a 2–3-nm-thick cPEG coating, as seen in Figure 1. The overall morphology of the nanoparticles synthesized in this manner is shown in the schematic image in Figure 1a. The reduction of the ferrous chloride produces FeNPs with the incorporation of interstitial boron that results from the reduction reaction. Using concentrated reagents and the reaction kinetics afforded by the simultaneous introduction of reagents in the junction, a highly uniform particle size distribution is obtained, as seen in Figure 1c, for the low-magnification bright-field transmission electron microscopy (TEM) image. Although the nanoparticles disperse well in solution, the clustering of particles seen was due to the magnetism and surface tension of the droplet on the carbon-coated TEM grid as it dries during preparation for imaging. When focusing on a single particle using high-resolution (HR) TEM as in Figure 1b, it becomes clear that the nanoparticles contain multiple components as evidenced by the three distinct levels of contrast. A crystalline core is surrounded by two amorphous shells with less contrast as a function of radius. Given the nature of the synthesis, it is highly likely that the first core is Fe with interstitial boron and the outer shell is the cPEG coating. The formation of borides using the borohydride reduction is strictly dependent on the concentration of the reagents[23] and since the concentrations are reduced as the reaction progresses, it is clear that more boron would be incorporated into the product as the nanoparticles nucleate and grow. From the selected-area electron diffraction (SAED) pattern in Figure 1d there are no reflections from iron boride phases. However, there is evident peak broadening in the α Fe reflections. This can be attributed to either the nanoscale particle size, resulting from Scherer broadening, or to the presence of an amorphous Fe component as boron is incorporated. We have found that as the nanoparticle size increases, X-ray line broadening is maintained due to an amorphous Fe-rich volume fraction present in the samples. Since it is well known that boron is a grain refiner, it is plausible that the boron is simply straining the iron lattice. The lighter amorphous shell is due to reduced Z contrast resulting from the low-molecular-weight cPEG that coats the nanoparticles compared to the amorphous iron boron. The reaction between the carboxyl group on the cPEG and the nanoparticle surface incorporates a slight oxide layer (FeO) that facilitates biocompatibility and prevents excessive oxidation of the nanoparticles. This layer accounts for the lighter reflections in the SAED pattern. The cPEG coating is stable in solution within a pH range of 5–8. Temperatures in excess of 70 °C can destroy the bond between the carbon and oxygen on the surface of the iron nanoparticle.

The higher magnetization and soft ferromagnetic nature shown by the novel FeNPs is evident from the magnetization curves shown in Figure 2 in comparison with one form of IONPs, which were Fe_3O_4 nanocrystals with a 10-nm core size and coated with amphiphilic triblock polymers (2–3 nm) prepared as previously described.[24,25] The FeNP saturation magnetization of 70 emu g^{-1} represents only a third of the bulk α-Fe value due to the nanoparticle size and the cPEG coating used. In addition to greater magnetization, the coercivity of the FeNPs is about 100 orders higher in comparison to IONPs, as shown in Figure 2. These two parameters are of central importance for biomedical applications such as MRI contrast enhancement and the induction of local hyperthermia for inducing cancer cell death.

By subjecting magnetic nanoparticles to an oscillating magnetic field, heat is generated in a highly localized manner. Heat generation is the result of eddy current, hysteresis, and Brownian-rotation loss mechanisms that all rely on the magnetic properties of the nanoparticle.[26] Increased magnetization afforded by the FeNPs allows for heat dissipation at frequencies in the safe range (<1.2 MHz) while for the IONPs much higher frequencies are required to facilitate the same thermal dose due to a higher FMR frequency. Hysteresis loss is directly proportional to the area enclosed by the magnetization curve. As seen in Figure 2, the hysteresis losses are enhanced in the FeNPs. This important advantage of FeNPs over IONPs is further demonstrated in Figure 3, comparing the heating curves of the FeNPs and the IONPs. There is a distinct difference in the achievable temperature between novel FeNPs and conventional IONPs at the same level of concentration. The concentration is measured by dissolving a known

mass of nanoparticles (including the nonmagnetic mass of polymer) with similar particle size distribution (mean size of 10 nm) in 2 mL of ethyl alcohol. Both ferro-fluids were excited with a 4 Oe, 500 kHz magnetic field. From these curves, it is evident that local hyperthermia is achievable with the FeNPs while IONPs require a dose in excess of 20-fold or greater to achieve the same temperature change.

To assess the relaxation properties and MRI contrast-enhancing effect of FeNPs, phantoms containing FeNPs at different concentrations were made as described in the Experimental Section. The longitudinal and transverse relaxivities, r_1 and r_2, respectively, were calculated from the measurement of T_1 and T_2 relaxation times of FeNPs at different concentrations at a magnetic field strength of 1.5 T on a clinical MRI scanner. The T_2 relaxation time was measured using a multiecho fast spin–echo sequence with 32 TE values ranging from 6 to 180 ms. The T_2 relaxation time of the FeNP sample was calculated by fitting the decay curve (Figure 4A) on a pixel-by-pixel basis using the nonlinear monoexponential algorithm of $M_{(TE)} = M_0 \cdot \exp(-TE/T_2)$. For the measurement of effective transverse relaxation time, T_2*, a dual-echo gradient-echo imaging sequence with susceptibility weighting was used to record images for a total of six echo times. T_2* values were obtained from the fit of the plot of MRI signal intensity versus echo times according to the equation: $M_{(TE)} — M_0 \cdot \exp(-TE/T2^*) + C$, where $M_{(TE)}$ is the signal intensity observed at a given echo time, TE, and C is a constant that reflects the background noise.

Table 1 summarizes the measurements of relaxivities r_1, r_2, and r_2*, which are defined as relaxation rates R_1, R_2, and R_2*, respectively, which are the reciprocal relaxation times (e.g., $R_1 = 1/T_1$) at the concentration unit and can be obtained from the slopes of the concentration versus relaxation time plots. Our data showed that r_2 and r_2* relaxivity of FeNPs is significantly higher than that of IONPs at a comparable particle size. Such a stronger T_2 shortening effect, typically from stronger magnetic susceptibility, leads to spin dephasing and substantial MRI signal drop, which generated a “darkening” contrast, as seen in T_2-weighted MRI images (Figure 4). Our results showed stronger T_2 shortening effects from FeNPs than IONPs suggesting that FeNPs have the potential to be more powerful contrast-enhancing media than currently used IONPs.

We believe that the FeNPs described in this report represent a new generation of magnetic nanoparticles that may serve as a multifunctional clinical tool. Based on their greater magnetization in comparison to conventional IONPs, these particles can serve as superior MRI contrast agents and can induce local hyperthermia. We have shown that elemental Fe-based nanoparticles may achieve high magnetism without the introduction of other metal elements that may be biologically toxic. Furthermore, the biocompatible cPEG coating of the FeNPs may allow for future covalent and stoichiometric attachment of bioactive ligands such as antibodies or receptor ligands specific to cancer cells providing surface functionalization and ultimate cell targeting. Magnetic targeting of tissues may also be possible due to the superior magnetic properties of these nanoparticles.

Experimental Section

FeNP synthesis and characterization

The reaction was carried out by reduction of the metal salt solution with a sodium borohydride solution.[20] $FeCl_2$ (2 g) was dissolved in ethyl alcohol (25 mL) and $NaBH_4$ (1 g) was dissolved in deionized water (25 mL). The reaction was carried out by mixing the two reagents through a Y junction in a closed system. The system is pressurized using nitrogen gas to pump the reagents through the Y tube and into the coating solution containing cPEG (10 mL) mixed with ethanol (50 mL). The reaction products were washed three times in ethyl alcohol and sonication was performed for 5 min. The magnetic nanoparticles are separated using a permanent magnet

and the liquid mixture is then poured off to get rid of dissolved byproducts such as NaCl and borides. The washed product was then stored in a vial of ethyl alcohol for measurements. A TEM (JEOL 3010) was used for particle size determination and microstructure.

Magnetic properties of FeNPs and IONPs

Magnetic properties were measured using a vibrating-sample magnetometer (Lake-Shore VSM) at room temperature with a maximum field of 1.0T.

Hyperthermia measurements

Heating characteristics were studied on the sample of IONPs or FeNPs dispersed in ethyl alcohol (2 mL) in a test tube seated in a ten-turn water-cooled copper coil by applying a 4 Oe and 500 kHz AC magnetic field. When suspended in ethyl alcohol and sonicated the particles formed a stable dispersion for a time period of 20 min, which was sufficient to perform the in vitro hyperthermia studies. Temperature measurements were made with an infrared temperature sensor connected to a digital thermometer located at the opening of the testtube and acquired data were normalized per unit mass for comparison.

MRI relaxometry

FeNPs or IONPs at given concentrations were suspended in an agarose gel (1%) and placed in tubes (10 mL).

Phantoms of different iron concentrations were made from stock solutions of IONPs and FeNPs. The atomic [Fe] concentrations of the stock solutions were determined using UV/Vis spectrophotometry. Typically, the nanoparticle samples were dissolved using high-concentration hydrochloride (HCl). The resulting solution was further reduced to Fe(II) before adding 1,10-phenanthroline monohydrate to form the colored complex. The [Fe] concentration was then determined by measuring the absorbance at 590 nm and calibration against the standard solutions. For T_1 measurement, an inversion recovery sequence was used with nine non-equidistant different time delays (T_I = 0.1–1 s) between inversion and the first 90 ° excitation pulse. A nonlinear curve fitting of the magnitude MRI signal intensity measured at different T_I time points from regions of interest (ROIs) selected in each sample to the equation of $M(T_I) = M_0 \times [1 - C \times \exp(-T_I/T_1)]$ (where T_I is inversion time and M is the magnitude of MRI signal), was used to calculate the T_1 relaxation time of each sample. For T_2 measurements, a multiecho fast spin–echo sequence was used to collect a series of data points simultaneously at different echo times (TEs of 6–180 ms with 6 ms increments). The T_2 relaxation time was measured using a multiecho fast spin–echo sequence with 32 TE values ranging from 6 to 180 ms. The T_2 relaxation time was calculated by fitting the decay curve using the nonlinear monoexponential algorithm of $M_{(TE)} = M_0 \exp(-TE/T_2)$.

References

1. Jain KK. Technol Cancer Res Treat 2005;4:407–416. [PubMed: 16029059]
2. Nasongkla N, Bey E, Ren J, Ai H, Khemtong C, Guthi JS, Chin SF, Sherry AD, Boothman DA, Gao J. Nano Lett 2006;6:2427–2430. [PubMed: 17090068]
3. Chertok B, David AE, Huang Y, Yang VC. J Controlled Release 2007;122:315–323.
4. Alexiou C, Arnold W, Klein RJ, Parak FG, Hulin P, Bergemann C, Erhardt W, Wagenpfeil S, Lubbe AS. Cancer Res 2000;60:6641–6648. [PubMed: 11118047]
5. Huh YM, Jun YW, Song HT, Kim S, Choi JS, Lee JH, Yoon S, Kim KS, Shin JS, Suh JS, Cheon J. J Am Chem Soc 2005;127:12387–12391. [PubMed: 16131220]
6. Bomati-Miguel O, Morales MP, Tartaj P, Ruiz-Cabello J, Bonville P, Santos M, Zhao X, Veintemillas-Verdaguer S. Biomaterials 2005;26:5695–5703. [PubMed: 15878375]

7. Neuwelt EA, Varallyay P, Bago AG, Muldoon LL, Nesbit G, Nixon R. Neuropathol Appl Neurobiol 2004;30:456–471. [PubMed: 15488022]
8. Shapiro EM, Skrtic S, Sharer K, Hill JM, Dunbar CE, Koretsky AP. Proc Natl Acad Sci USA 2004;101:10901–10906. [PubMed: 15256592]
9. Slotkin JR, Cahill KS, Tharin SA, Shapiro EM. Neurotherapeutics 2007;4:428–433. [PubMed: 17599708]
10. Lee JH, Huh YM, Jun YW, Seo JW, Jang JT, Song HT, Kim S, Cho EJ, Yoon HG, Suh JS, Cheon J. Nat Med 2007;13:95–99. [PubMed: 17187073]
11. McCarthy JR, Kelly KA, Sun EY, Weissleder R. Nanomedicine 2007;2:153–167. [PubMed: 17716118]
12. Lewin M, Carlesso N, Tung CH, Tang XW, Cory D, Scadden DT, Weissleder R. Nat Biotechnol 2000;18:410–414. [PubMed: 10748521]
13. Moore A, Marecos E, Bogdanov A Jr, Weissleder R. Radiology 2000;214:568–574. [PubMed: 10671613]
14. Hilger I, Kiebling A, Romanus E, Hiergeist R, Hergt R, Andra W, Roskos M, Linss W, Weber P, Weitschies W, Kaiser WA. Nanotechnology 2004;15:1027–1032.
15. Campbell RB. Nanomedicine 2007;2:649–652. [PubMed: 17976026]
16. Johannsen M, Gneveckow U, Eckelt L, Feussner A, Waldofner N, Scholz R, Deger S, Wust P, Loening SA, Jordan A. Int J Hyperther 2005;21:637–647.
17. Pankhurst QA, Connolly J, Jones SK, Dobson J. J Phys D: Appl Phys 2003;36:R167–R181.
18. Luderer AA, Borrelli NF, Panzarino JN, Mansfield GR, Hess DM, Brown JL, Barnett EH, Hahn EW. Radiat Res 1983;94:190–198. [PubMed: 6856765]
19. Chan DCF, Kirpotin DB, Bunn PA. J Magn Magn Mater 1993;122:374–378.
20. Hergt R, Andra W, Ambly CG, Hilger I, Kaiser WA, Richter U, Schmidt HG. IEEE Trans Magn 1998;34:3745–3754.
21. Zhang Y, Kohler N, Zhang M. Biomaterials 2002;23:1553–1561. [PubMed: 11922461]
22. Bonder MJ, Gallo D, Srinivasan B, Hadjipanayis GC. IEEE Trans Magn 2007;43:2457–2458.
23. Glavee GN, Klabunde KJ, Sorensen CM, Hadjipanayis GC. Inorg Chem 1995;34:28–35.
24. Kim M, Chen Y, Liu Y, Peng X. Adv Mater 2005;17:1429–1432.
25. Gao X, Cui Y, Levenson RM, Chung LWK, Nie S. Nat Biotechnol 2004;22:969–976. [PubMed: 15258594]
26. Rosensweig RE. J Magn Magn Mater 2002;252:370–374.

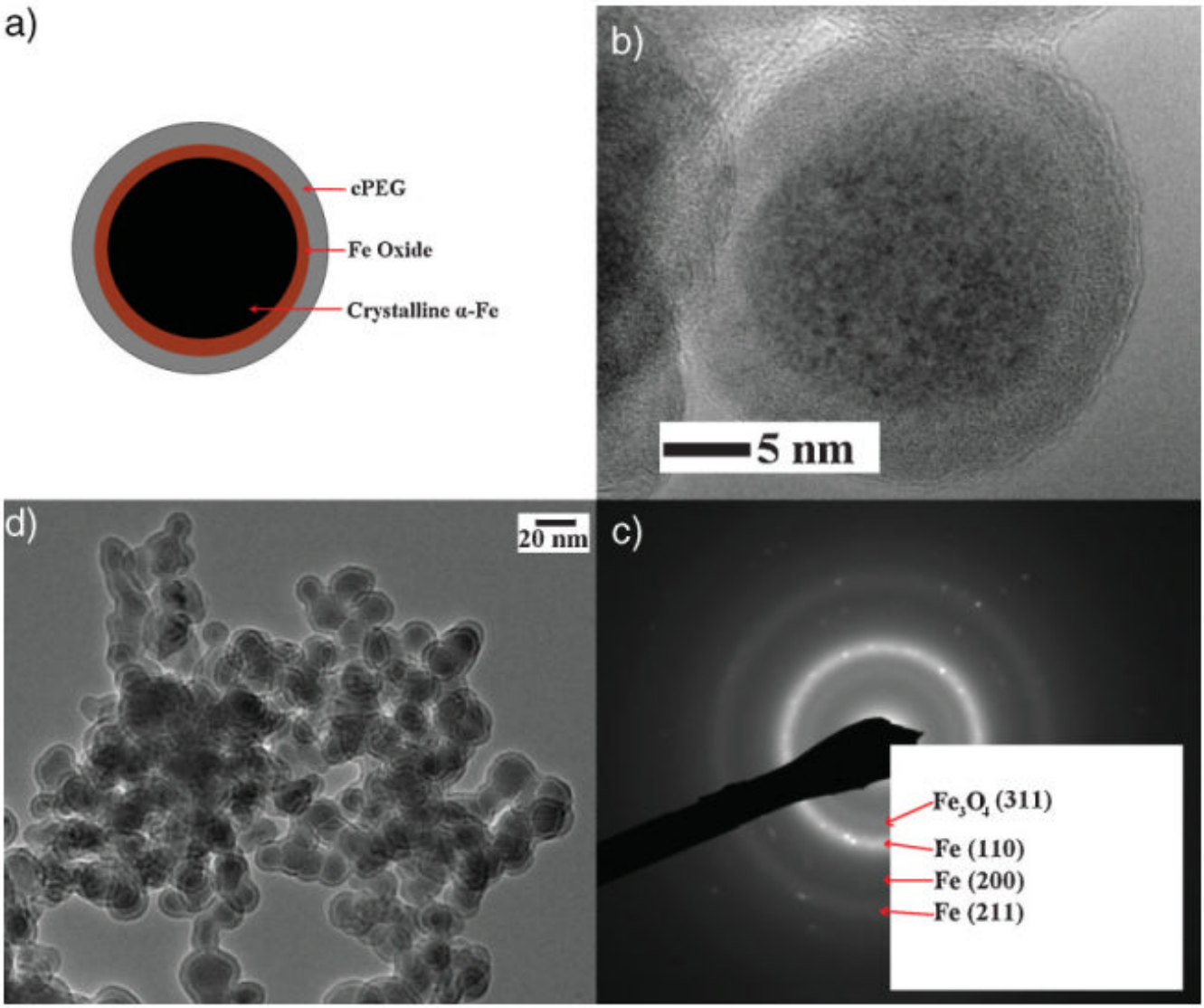

Figure 1.
Transmission electron microscopy data: a) schematic image of the polymer-coated Fe-based metallic nanoparticles, b) high-resolution image, c) bright-field image showing coated FeNPs. d) SAED image confirming the body-centered cubic (bcc) structure of α Fe together with a small amount of FeO.

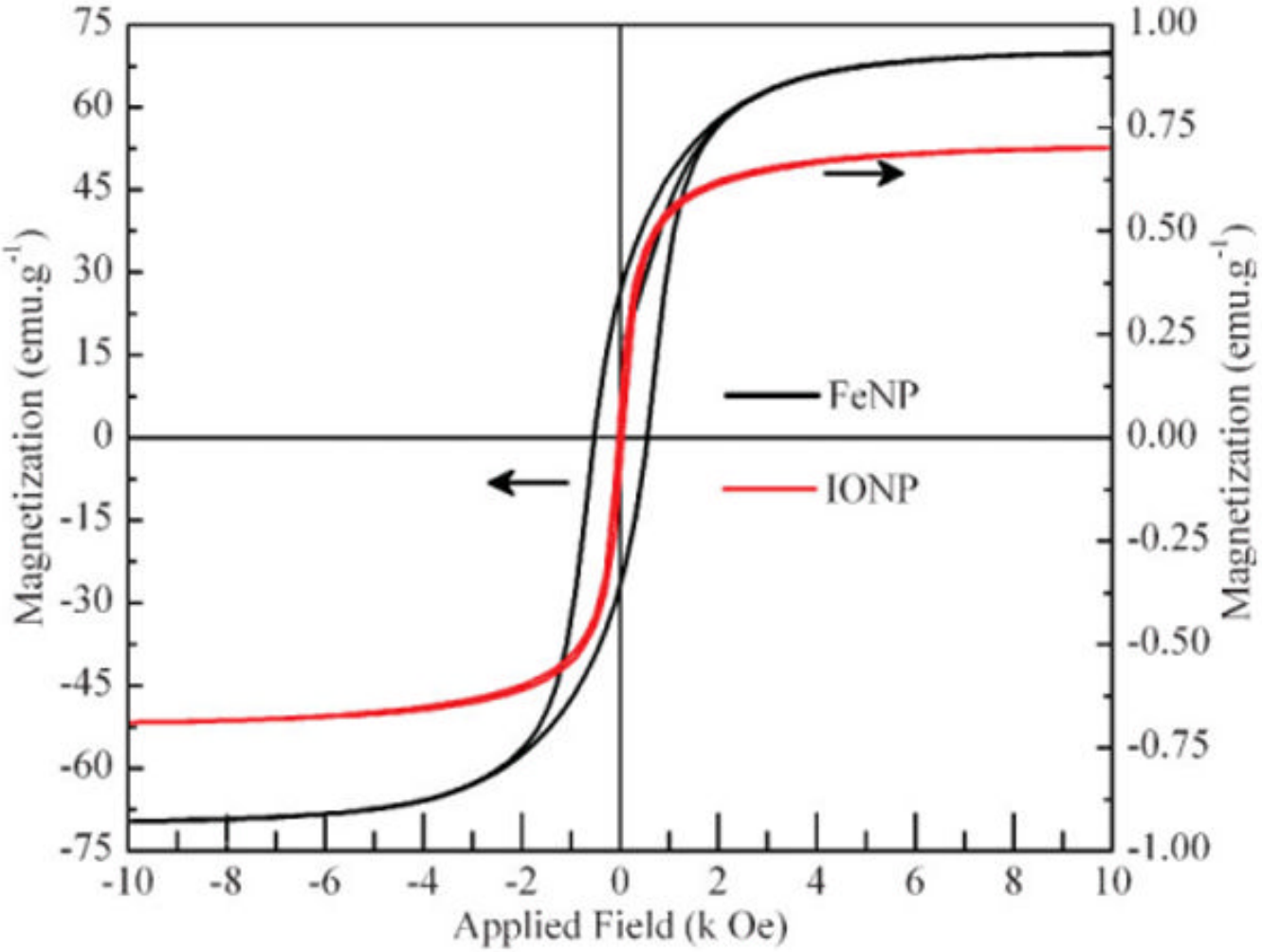

Figure 2.
Hysteresis loops for FeNP and IONP taken at room temperature.

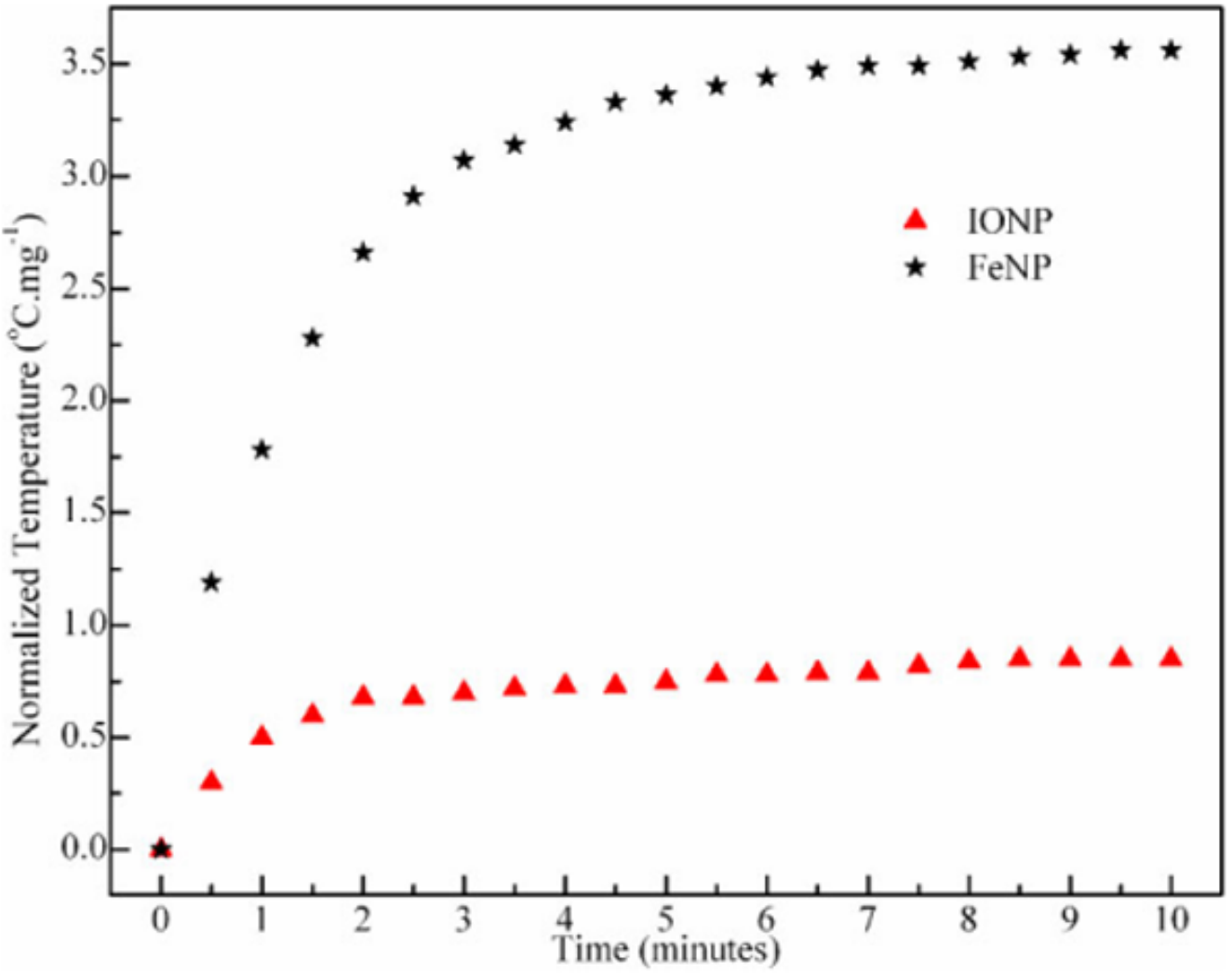

Figure 3.
Hyperthermia data for FeNPs and IONPs using 500 MHz and 4 Oe AC magnetic field.

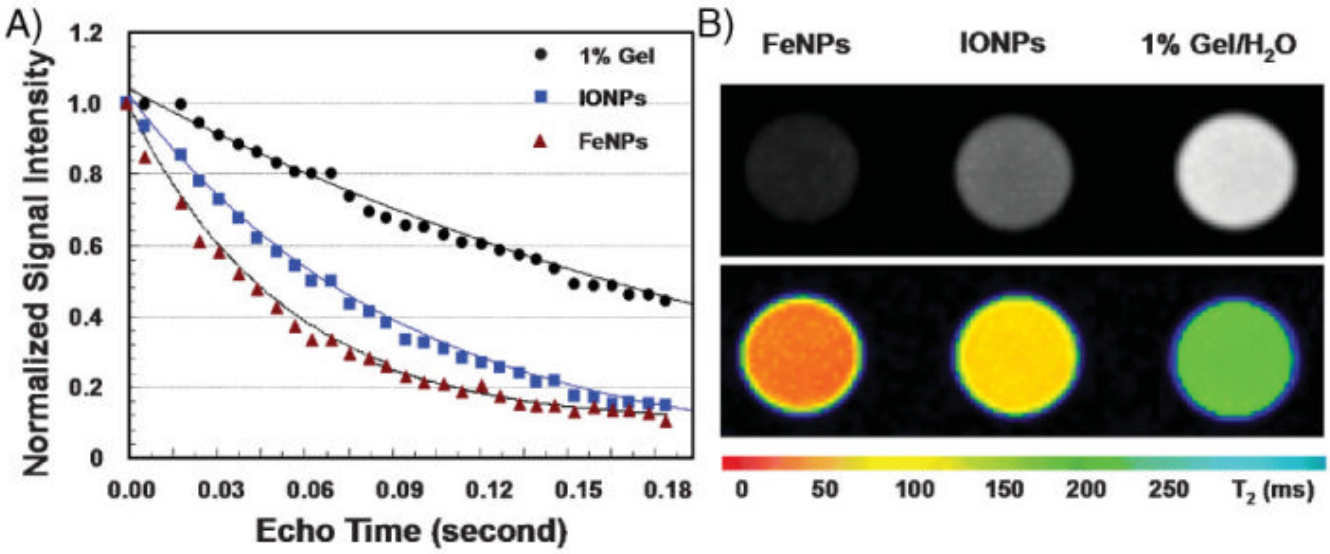

Figure 4.

Decreasing signal density at different echo times showed typical paramagnetic-induced T_2 decay in different samples (A). A set of T_2-weighted fast spin–echo images showed the strong T_2 contrast from FeNPs and IONPs (darkening effect) in contrast to the H_2O phantom (B, upper panel) while a T_2 relaxometry map derived from the multi-TE T_2 measurement showed a substantially lower T_2 value of the FeNPs (B, lower panel). T_2 images were recorded using a multi-TE fast spin–echo imaging sequence with a TR of 3 s and 32 TE points (starting at 6 ms with increments of 6 ms). The sample concentrations of IONPs and FeNPs shown in the Figure are 0.11 and 0.12 mM, respectively.

Table 1

Relaxivities of FeNPs and IONPs, measured at 1.5 T with contrast agents suspended in 1% agarose gel.

	Deionized H_2O	Gd-DTPA	FeNPs	IONPs[a]
r_1 (s^{-1} mM^{-1})	0.01±0.002	6.2±0.24	1.2±0.23	15.2±1.1
r_2 (s^{-1} mM^{-1})	0.54±0.12	8.2±0.36	129±5.9	56±2.1
r_2* (s^{-1} mM^{-1})	0.43±0.11	–	112±3.4	54±2.3

[a] Data from the IONP with core size of 10 nm.